

Inverse Model-Based Real-Time Control for Temperature Uniformity of RTCVD

Artemis Theodoropoulou, Evangelos Zafiriou, *Member, IEEE*, and Raymond A. Adomaitis

Abstract—A reduced-order model describing a rapid thermal chemical vapor deposition (RTCVD) process is utilized for real-time model based control for temperature uniformity across the wafer. Feedback is based on temperature measurements at selected points on the wafer surface. The feedback controller is designed using the internal model control (IMC) structure, especially modified to handle systems described by ordinary differential and algebraic equations. The IMC controller is obtained using optimal control theory on singular arcs extended for multi-input systems. Its performance is also compared with one based on the Hirschorn inverse of the model. The proposed scheme is tested with extensive simulations where the full-order model is used to emulate the process. Several cases of significant uncertainty, including model parameter errors, process disturbances, actuator errors, and measurement noise are used to test the robustness of the controller to real life situations. Both controllers succeed in achieving temperature uniformity well within the desirable bounds, even in cases where several sources of uncertainty are simultaneously present with measurement noise.

Index Terms—Internal model control, process control, RTCVD.

NOMENCLATURE

A	Discretization array (first derivative).
B	Discretization array (Laplacian operator).
C_{pw}	Wafer specific heat.
$Q_{dw,b}$	Radiative energy to the wafer bottom surface.
$Q_{dw,t}$	Radiative energy to the wafer top surface.
Q_{edge}	Wafer edge incident radiation flux.
$Q_{lamps,w}$	Radiant energy flux from the lamp banks to the wafer.
r	Radial coordinate.
R_w	Wafer radius.
t	Time.
T	Wafer temperature.
T_{amb}	Ambient temperature.
T_c	Chamber temperature.
T_{des}	Desired temperature.
u_A, u_B, u_C	Lamp bank power percentage.

ϵ_w	Emissivity of the wafer.
κ	Wafer conductivity.
ρ_w	Wafer density.
σ	Boltzmann constant.

I. INTRODUCTION

FIRST principle models can generally be developed to describe the thermal dynamics of a rapid thermal chemical vapor deposition (RTCVD) reactor in an accurate manner. Such models, however, cannot be directly used in designing and implementing real-time model based controllers, due to their distributed parameter nature. Also the large size of their lumped parameter approximations can result in prohibitive computational demands. A simple nonlinear lumped parameter model is used in [1] for run-to-run control of the wafer temperature, but it does not describe the process in terms of spatial uniformity. In [2] an improved distributed parameter dynamic model is developed, and then lumped in order to be used for nonlinear model predictive control. A model reduction technique is proposed in [3] to reduce the size of the initial lumped parameter approximation. Thus one can obtain a reduced-order nonlinear model with good predictive capabilities, that is also of a form and size suitable for control and optimization of the process. Several papers in the literature utilize linear control and estimation techniques for temperature control in rapid thermal processing (e.g., [4] and [5]).

In this paper we consider the RTCVD system described in [3] and [6] with the goal of designing a nonlinear model based real-time control system for temperature uniformity that is robust with respect to several types of modeling uncertainties and process disturbances. The process model equations are affine to the three inputs (power of lamp zones) giving rise to a singular optimal control problem. Single-input singular optimal control problems have been studied extensively by [7] and used for optimization and control in several cases of biochemical single-input systems [8], [9]. A state feedback formulation using geometric methods has also been developed in [10]. Since the RTCVD reactor we consider is a multi-input system, we had to develop in this paper optimal control law formulations for the multi-input case.

The theory that we develop is used to obtain feedback optimal control laws for the singular region of operation. This controller is compared with one based on the Hirschorn inverse [11]. Both controllers use the reduced-order model developed in [3]. The controllers are implemented in the internal model control (IMC) structure [12], modified to enable handling of differential/algebraic equation systems. Several cases of model

Manuscript received October 1, 1997; revised August 15, 1998. This work was supported by the National Science Foundation through Grants NSF CTS-9057292 and NSF EEC-9527576.

A. Theodoropoulou was with the Department of Chemical Engineering and Institute for Systems Research, University of Maryland, College Park, MD 20742 USA. She is now with OSI Software, Inc., San Leandro, CA 94577 USA (e-mail: atheodor@osisoft.com).

E. Zafiriou and R. A. Adomaitis are with the Department of Chemical Engineering and Institute for Systems Research, University of Maryland, College Park, MD 20742 USA (e-mail: zafiriou@isr.umd.edu; adomaiti@isr.umd.edu).

Publisher Item Identifier S 0894-6507(99)01220-8.

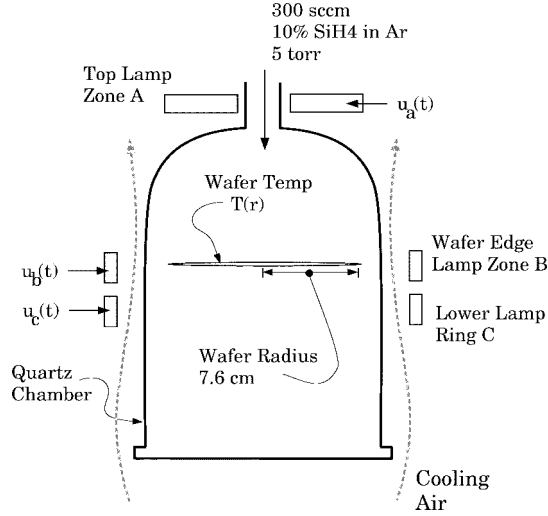


Fig. 1. NCSU RTCVD system.

TABLE I
COLLOCATION POINTS FOR THE FOUR-POINT FORMULATION

Point	r
1	0
2	0.4388
3	0.9076
4	1

uncertainty and disturbances are considered in order to test the robustness of the performance of both controllers. The predictive capabilities of the model reduction method of [3], that were so far only tested for steady state optimization, are now evaluated for the dynamic optimization and control case.

II. PROCESS DESCRIPTION AND MODEL

The system we consider is based on the three-zone RTCVD reactor located at the North Carolina State University (NCSU) Center for Advanced Electronic Materials Processing [6]. A diagram is shown in Fig. 1. A 10% silane feed in inert gas enters the reactor from the top. The silane decomposes to silicon and hydrogen. The goal of the process is the uniform deposition of a 0.5- μm film of polysilicon on the wafer. Polysilicon deposition occurs at temperatures of approximately 800K or higher and the heating of the wafer is accomplished by controlling the power to the three zones of lamp banks. As described in [13], maintaining the pressure constant at 5 torr, the wafer is heated until a preset temperature is reached. The process temperature remains constant for a preprogrammed amount of time, after which the valve to the reactant feed is closed and the lamp power supply is turned off. The pressure is then increased so that the system can cool down quickly.

Detailed modeling of this process has been done in [3]. Definition of the various symbols is given in the Nomenclature section. (Boldface symbols are used to indicate arrays.) The model consists of a nonlinear partial differential equation describing the wafer temperature, in the form

$$\frac{\partial T(t, r)}{\partial t} = f_w(r, T, T_c) + \mathbf{g}_w(r) \cdot \mathbf{U}(t) \quad (1)$$

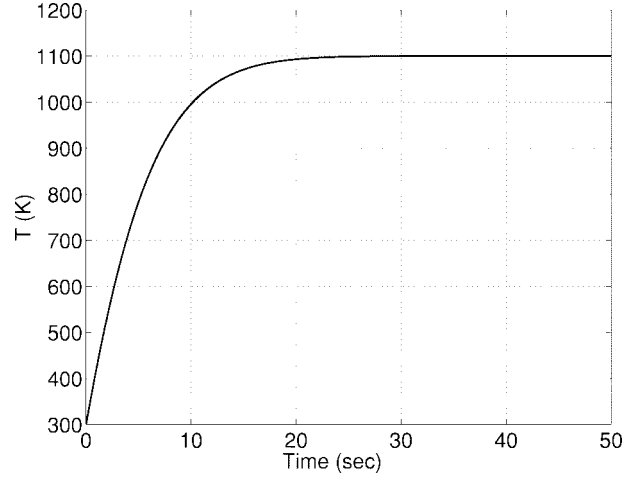


Fig. 2. The wafer temperature setpoint profile.

where

$$\mathbf{U} = [u_A \ u_B \ u_C]^T.$$

There are two nonlinear boundary conditions:

$$\left. \frac{\partial T}{\partial r} \right|_{r=0} = 0, \quad (2)$$

$$\left. \frac{\partial T}{\partial r} \right|_{r=1} = h_1(T, T_c) + k_1(T)u_B. \quad (3)$$

The model also includes a lumped ordinary differential equation approximating the chamber temperature dynamics in the form

$$\frac{dT_c}{dt} = f_c(T, T_c) + \mathbf{g}_c \cdot \mathbf{U}(t). \quad (4)$$

The detailed expressions of the several terms in (1)–(4) can be found in [3]. Specifically (1) corresponds to (2) and (5) in [3], (3) to (4) in [3], and (4) to (11) in [3]. A discretized full-order model was used for simulation purposes. The wafer temperature was discretized at 76 uniformly-spaced points, thus giving a nonlinear state space model with 77 state variables including the chamber temperature T_c . The distributed parameter model cannot be directly utilized in model based control due to its form. Even in the discretized form it is not computationally efficient and definitely not handy for model based control, since it involves such a large number of states. This was, indeed, the motivation for the development of the model reduction procedure presented in [3]. In that work application of this technique to the detailed model described by (1)–(4) above, resulted in a model of the form

$$\frac{d\mathbf{T}}{dt} = \mathbf{f}_r(\mathbf{T}, T_4) + \mathbf{g}_r \cdot \mathbf{U}(t) \quad (5)$$

$$h(\mathbf{T}, T_4) + ku_B = 0 \quad (6)$$

where

$$\mathbf{T} = [T_1 \ T_2 \ T_3 \ T_c]^T \quad (7)$$

and T_1, T_2, T_3, T_4 are the temperatures corresponding to four collocation points across the radius of the wafer. The detailed

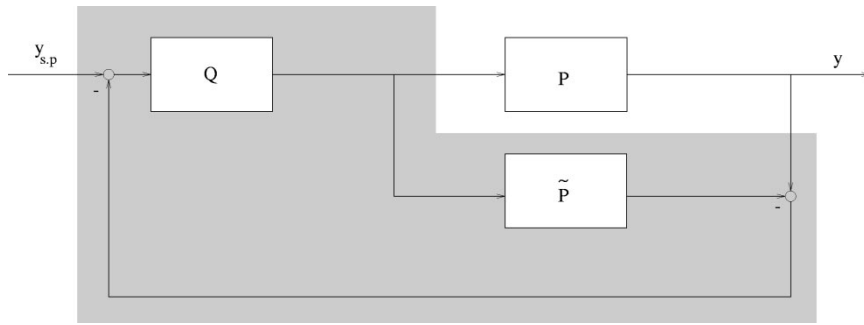


Fig. 3. The standard IMC structure.

expressions for (5) and (6) can be found in [3] from (38) and (39) of that reference.

In [3], six collocation points [14] were used for the discretization of the system. We repeated the model reduction procedure using only four collocation points for two reasons. First, this number enables the creation of the control law we propose in the following sections. Second, we wanted to check the robustness of the proposed control scheme even when the reduced-order model was not the most precise. The analytical expression and discretization matrices of the four-point reduced-order model are given in the Appendix. The collocation points for the four-point reduced-order model are given in Table I. The first point corresponds to the wafer center and the fourth to the edge.

The reduced-order model consists of a set of four ordinary differential equations and one algebraic equation, and it is suitable for real-time control of the process. It should also be pointed out that, in this form, (5) is the state space representation of a nonlinear system which is *affine* with respect to the input \mathbf{U} . This is a very important characteristic of the system from a control point of view, and it will remain present even if elements of the reactor design like reactor size or location of lamp banks change.

III. CONTROL PROBLEM FORMULATION

A. Control Objective

The objective of the process is to achieve uniform deposition thickness of polysilicon of $0.5 \mu\text{m}$ along the wafer surface. Based on the assumption of constant emissivity in [3], the model equations describing the wafer temperature and those describing the deposition thickness are decoupled. Since the spatial dependence of the deposition thickness is due to the wafer temperature spatial dependence, we pursue our initial objective indirectly, aiming for uniform wafer temperature that will result in the desirable deposition thickness. Hence, we use only the temperature equations in the controller design. In reality, emissivity is not constant. Nevertheless, temperature uniformity is expected to be sufficient for deposition thickness uniformity. Furthermore, the controller is designed to be robust with respect to such process model error. Suitable tests have been done allowing the emissivity to vary, and they are included in Section V-A.

In order to choose the wafer temperature setpoint profile, shown in Fig. 2, we performed simulations that use the de-

position thickness model equations described in [3]. Using this temperature setpoint, the necessary run time for $0.5 \mu\text{m}$ deposition was determined to be 50 s. Nevertheless, even if there are errors in the kinetics model, the closed-loop formulation would allow us to determine the necessary run time by use of an end-point sensor that measures the deposition thickness. Accordingly, the run would stop when the measured deposition thickness had reached the desired level.

Furthermore, one should note that according to the SIA National Technology Roadmap for Semiconductors [15] the maximum acceptable temperature nonuniformity can be up to 5K.

B. Nonlinear Internal Model Control

The feedback controller design is done using internal model control (IMC) [16]. The IMC structure is presented schematically in Fig. 3. The classic feedback controller C is represented by the shaded area. P is the process under consideration and \tilde{P} the model describing the process. When using the IMC structure, one designs the IMC controller Q and, then, implements it combined with the model \tilde{P} as shown in Fig. 3.

IMC has a very important property [12]. If the IMC controller is equal to the model inverse ($Q = \tilde{P}^{-1}$), and the closed loop system in Fig. 3 is stable, then $y(t) = y_{sp}(t)$ for all $t > 0$ and all disturbances $d(t)$. This property is known as *perfect control*.

In the past, the IMC structure has been extended for nonlinear systems [12]. However, the existence of the algebraic equation (6) in the model obstructs the application of standard nonlinear IMC for this system. This has led us to modify the IMC formulation, making it suitable for dealing with several specific systems described by differential and algebraic equation models.

The fact that (6) is nonlinear with respect to the edge temperature T_4 prevents us from solving analytically for T_4 . On the other hand, since it is linear with respect to the input u_B , it can be solved yielding u_B as a function of \mathbf{T} and T_4 . Furthermore, if T_4 is set to be equal to the setpoint value, one can substitute for u_B in (5) transforming it to

$$\frac{d\mathbf{T}}{dt} = \mathbf{f}(\mathbf{T}, T_{des}) + \mathbf{g} \cdot \mathbf{u}(t) \quad (8)$$

where

$$\mathbf{u} = [u_A \ u_C]^T \quad (9)$$

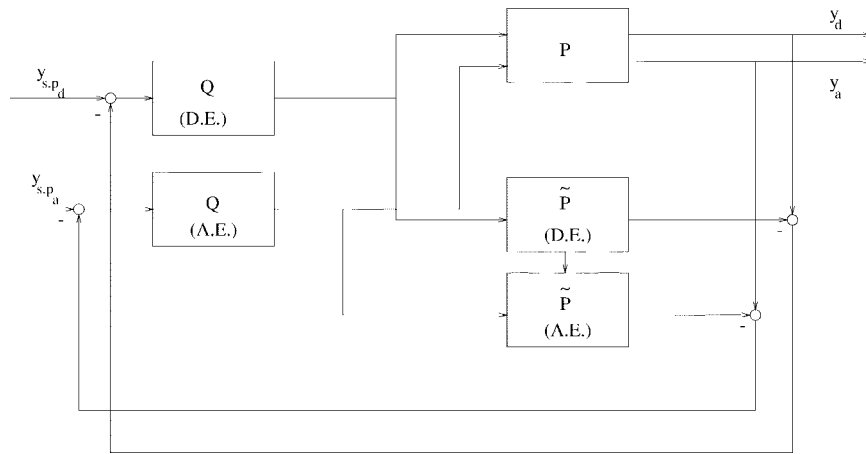


Fig. 4. The modified IMC structure.

\mathbf{g} consists of the first and the third column of \mathbf{g}_r and \mathbf{f} is formed by algebraic manipulations involving the substitution of u_B from the solution of (6). This way the differential equations are decoupled from the algebraic equation for the purpose of controller design.

In the modified IMC structure, shown in Fig. 4, IMC is applied separately to the differential equations and to the algebraic equation. We denote with y_d the output of the process that corresponds to the differential equations of the model, and with y_a the output of the process that corresponds to the algebraic equation of the model. For our system $y_a = T_4$ but y_d depends on which inner temperatures we choose to control as explained in Section III-A. As a result of this decoupling, the edge temperature T_4 is controlled directly by u_B and the inner temperature points are controlled by the remaining inputs u_A and u_C . Even though the controller equations are completely decoupled, the algebraic model equation is still (6) and it requires the use of values for the states, which is indicated by the arrow from $\tilde{P}(D.E.)$ to $\tilde{P}(A.E.)$ in Fig. 4.

IV. CONTROLLER DESIGN

In order to use the modified IMC structure we need to design a separate controller for the edge temperature, which is described by the algebraic equation (6), and one for the inner temperature point dynamics, described by the quasi-linear two-input system (8).

Standard inverse model based controller design requires a square system, where the number of controlled outputs is the same as that of the manipulated inputs. To apply such techniques on (8), we need to select for control only two of the three inner temperature points. We do so by using the Hirschorn inverse in Section IV-B.

In order to control all three inner temperatures of system (8) we designed a controller based on optimal control theory on singular arcs. Since we have two inputs we need to extend some of the existing single-input theory to the multi-input case. The method is described in Section IV-C.

In both cases, the controller used for the edge temperature control is the same and it is presented in Section IV-A.

A. Edge Temperature Control

In order to benefit it from the perfect control property of IMC, we need to invert the algebraic equation (6). We do this simply by solving (6) for u_B . Since T_4 is the controlled variable, it has to be substituted by the feedback signal $T_{des} - (T_4 - \tilde{T}_4)$. Thus,

$$u_B = -\frac{h(\tilde{\mathbf{T}}, T_{des} - (T_4 - \tilde{T}_4))}{k}. \quad (10)$$

Equation (10) must be consistent with (6), and so we must use the model prediction values \tilde{T}_i for the remaining temperature points T_1 , T_2 , and T_3 , which is indicated by the use of $\tilde{\mathbf{T}}$ in (10). In cases, where (10) would result in values of u_B violating the lower limit of zero, the value is set to be equal to zero. The upper limit of one would be treated similarly, but that limit was never violated during simulations by the solution of (10).

B. Hirschorn Inversion

For square, quasi-linear systems the Hirschorn inverse formula [11], [17], can be applied. For this to be possible with the system described by (8), we have to choose only two of the three temperatures as the output of the system, so that our system is square. After performing simulations with all the combinations, we decided to use temperatures T_1 and T_2 , since there was no difference in choosing one combination versus another. Our system now is described by (8) and the output equation

$$\mathbf{y}_d = \begin{bmatrix} y_1 \\ y_2 \end{bmatrix} = \begin{bmatrix} 1 & 0 & 0 & 0 \\ 0 & 1 & 0 & 0 \end{bmatrix} \cdot \begin{bmatrix} T_1 \\ T_2 \\ T_3 \\ T_c \end{bmatrix} = \mathbf{C} \cdot \mathbf{T}. \quad (11)$$

Control analysis performed on a linearization of (8), obtained at an operating point corresponding to the final temperature values of the trajectory shown in Fig. 2, shows no unstable zeros [16] for the 2×2 transfer function matrix. This indicates that the inverse model is at least locally stable. Application of the Hirschorn inversion on the system described

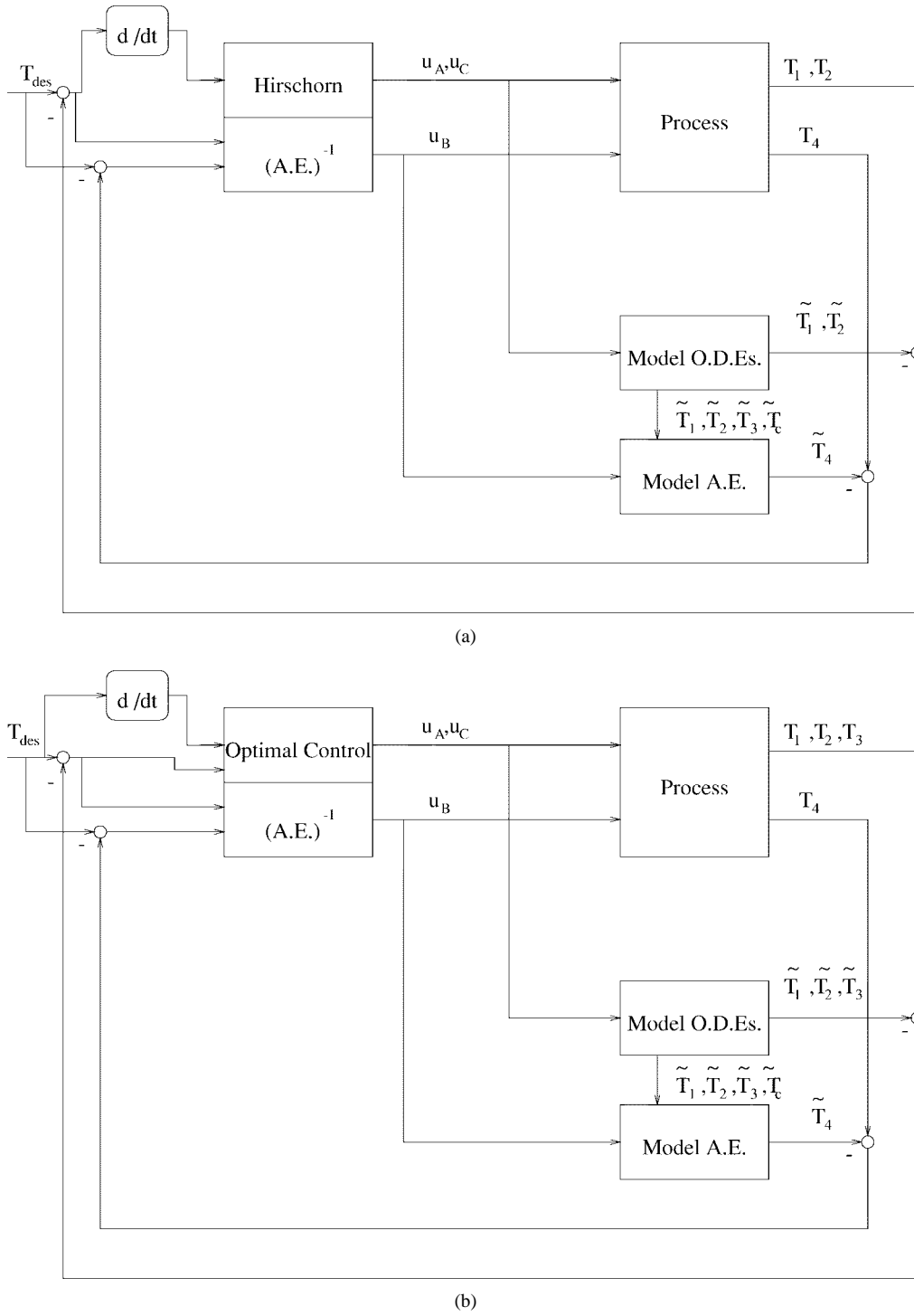


Fig. 5. Implementation of the two controllers in IMC structure: (a) Hirschorn inverse and (b) singular optimal control law.

by (8) and (11) yields

$$\dot{\mathbf{Z}} = \mathbf{f}(\mathbf{Z}) + \mathbf{g}(\mathbf{Z})(L_g L_f^{r-1}(\mathbf{C} \cdot \mathbf{Z}))^{-1} \cdot \left(\frac{d^r \mathbf{y}}{dt^r} - L_f^r(\mathbf{C} \cdot \mathbf{Z}) \right) \quad (12)$$

$$\mathbf{u} = (L_g L_f^{r-1}(\mathbf{C} \cdot \mathbf{Z}))^{-1} \cdot \left(\frac{d^r \mathbf{y}}{dt^r} - L_f^r(\mathbf{C} \cdot \mathbf{Z}) \right) \quad (13)$$

where L_f and L_g are Lie derivative operators [17], defined as

$$L_f = \sum_{i=1}^n f_i(x) \frac{\partial}{\partial x_i} \quad (14)$$

and r is the relative order of the system [17], defined as the smallest integer for which

$$L_g L_f^{r-1}(\mathbf{C} \cdot \mathbf{Z}) \neq 0.$$

Equation (12) is the state-space description of the inverse model and (13) gives the output of the inverse model which

will serve as the control input of the actual system. \mathbf{Z} denotes the state vector of the model inverse and it corresponds physically to vector \mathbf{T} , having also the same initial conditions.

For this system we have calculated r to be 1, so after algebraic manipulations (12) and (13) become

$$\dot{\mathbf{Z}} = \mathbf{f}(\mathbf{Z}) + \mathbf{g}(\mathbf{C} \cdot \mathbf{g})^{-1} \left(\frac{d\mathbf{y}_d}{dt} - \mathbf{C} \cdot \mathbf{f}(\mathbf{Z}) \right) \quad (15)$$

$$\mathbf{u} = (\mathbf{C} \cdot \mathbf{g})^{-1} \left(\frac{d\mathbf{y}_d}{dt} - \mathbf{C} \cdot \mathbf{f}(\mathbf{Z}) \right). \quad (16)$$

For the implementation of (15) and (16) in the IMC structure of Fig. 4, \mathbf{y}_d at each time should be set equal to

$$\mathbf{y}_d = \begin{bmatrix} T_{des} - (T_1 - \tilde{T}_1) \\ T_{des} - (T_2 - \tilde{T}_2) \end{bmatrix}. \quad (17)$$

C. Optimal Control on the Singular Arc Region

In order not to limit the control action to only two of the three inner temperature points, we applied optimal control theory to the design of a model based controller. The fact that the model equation (5) is affine in \mathbf{U} results in a singular solution [18]. Under certain conditions, this open-loop solution can be transformed into a static state feedback control formulation suitable for closed-loop implementation. For the case of single-input systems this development can be found in [10]. The extension to multi-input systems that we present in this section is a new theoretical contribution on the subject.

Our objective is for each of the temperature points to track the desired temperature $T_{des}(t)$. This can be expressed as

$$\min_{\mathbf{u}} J = \int_0^{t_f} ((T_1 - T_{des})^2 + (T_2 - T_{des})^2 + (T_3 - T_{des})^2) dt \quad (18)$$

subject to (8), where t_f denotes the final time of the process. We choose to use the temperature points instead of the amplitude coefficients that we have used in [3], because, since this is a closed-loop formulation, it is more convenient to use outputs that can be measured directly.

For the solution of (18) we need to form the Hamiltonian of the system

$$H = \boldsymbol{\lambda}^T \mathbf{f} + \boldsymbol{\lambda}^T \mathbf{g} \mathbf{u} + L \quad (19)$$

where the elements of the vector $\boldsymbol{\lambda}$ of dimension 4 are the adjoint states of the system, and

$$L = (T_1 - T_{des})^2 + (T_2 - T_{des})^2 + (T_3 - T_{des})^2. \quad (20)$$

The necessary optimality conditions [18] are

$$H_{\mathbf{u}} = \boldsymbol{\lambda}^T \mathbf{g} = 0 \quad (21)$$

$$\dot{\boldsymbol{\lambda}}^T = -H_{\mathbf{T}} = -\boldsymbol{\lambda}^T \mathbf{f}_{\mathbf{T}} - L_{\mathbf{T}} \quad (22)$$

$$\boldsymbol{\lambda}(t_f) = 0 \quad (23)$$

where the subscripts denote partial derivatives. Because the Hamiltonian is linear in the control, \mathbf{u} , the optimal control problem is *singular* [10]. For a singular $\mathbf{u}(t)$ we have that

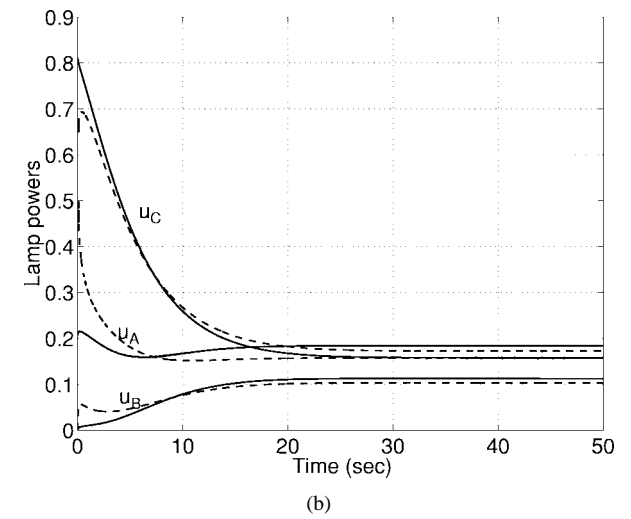
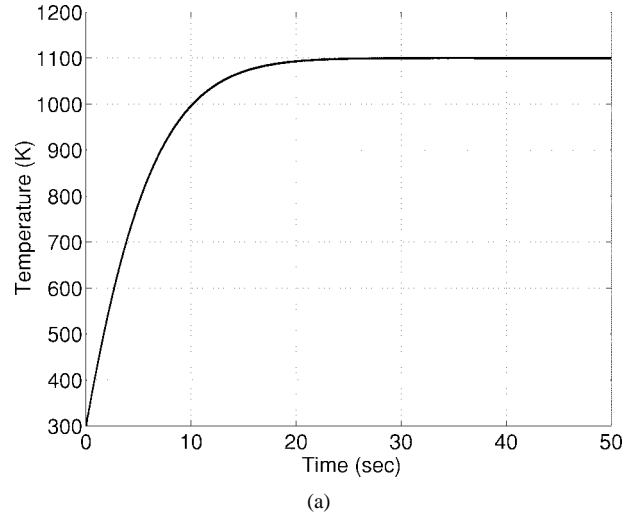


Fig. 6. IMC dynamic behavior using the full-order model as the simulated process and the reduced-order model as the model: (a) process output (temperature) and (b) manipulated inputs (lamp powers). Solid line: singular optimal control law. Dashed line: Hirschorn inverse.

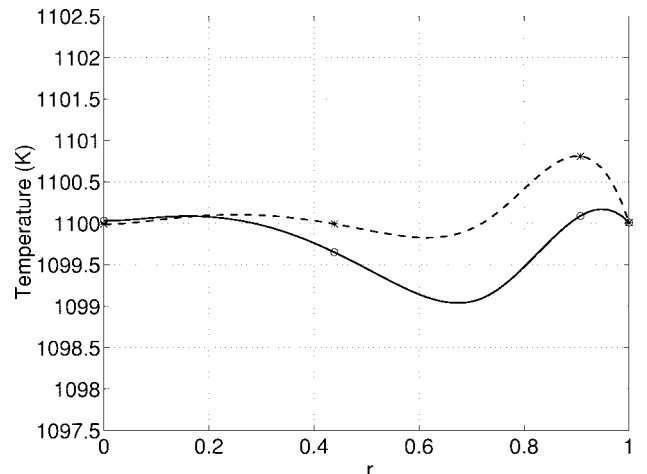


Fig. 7. Temperature profiles at final time using the full-order model as the simulated process and the reduced-order model as the model. Solid line: singular optimal control law. Dashed line: Hirschorn inverse.

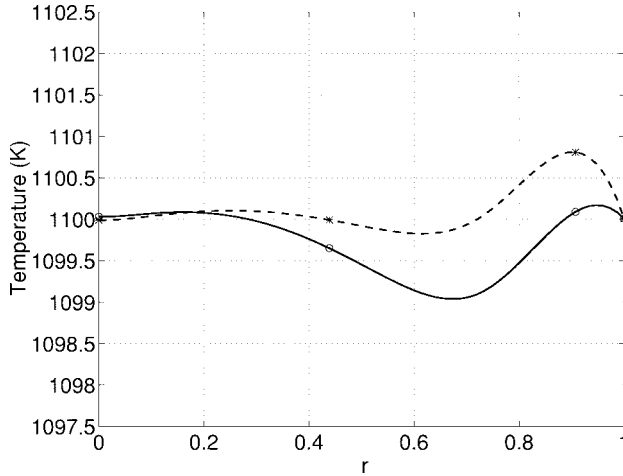


Fig. 8. IMC formulation using the full-order model as the simulated process with disturbance up to 10K in the wafer temperature and the reduced-order model as the model. Detailed temperature profile at $t = 50$ s. Solid line: singular optimal control law. Dashed line: Hirschorn inverse.

$H_{\mathbf{u}} = 0$ for all times; therefore its successive time derivatives are also zero. Thus

$$\frac{dH_{\mathbf{u}}}{dt} = \dot{\lambda}^\top \mathbf{g} = -\lambda^\top \mathbf{f}_{\mathbf{T}} \mathbf{g} - L_{\mathbf{T}} \mathbf{g} = 0 \quad (24)$$

$$\begin{aligned} \frac{d^2 H_{\mathbf{u}}}{dt^2} &= -\dot{\lambda}^\top \mathbf{f}_{\mathbf{T}} \mathbf{g} - \lambda^\top \frac{\partial(\mathbf{f}_{\mathbf{T}} \mathbf{g})}{\partial \mathbf{T}} \dot{\mathbf{T}} - \lambda^\top \frac{\partial(\mathbf{f}_{\mathbf{T}} \mathbf{g})}{\partial T_{des}} \dot{T}_{des} \\ &\quad - \frac{\partial(L_{\mathbf{T}} \mathbf{g})}{\partial \mathbf{T}} \dot{\mathbf{T}} - \frac{\partial(L_{\mathbf{T}} \mathbf{g})}{\partial T_{des}} \dot{T}_{des} \\ &= \lambda^\top \mathbf{f}_{\mathbf{T}}(\mathbf{f}_{\mathbf{T}} \mathbf{g}) + L_{\mathbf{T}}(\mathbf{f}_{\mathbf{T}} \mathbf{g}) - \lambda^\top \frac{\partial(\mathbf{f}_{\mathbf{T}} \mathbf{g})}{\partial \mathbf{T}} \dot{\mathbf{T}} \\ &\quad - \lambda^\top \frac{\partial(\mathbf{f}_{\mathbf{T}} \mathbf{g})}{\partial T_{des}} \dot{T}_{des} - \frac{\partial(L_{\mathbf{T}} \mathbf{g})}{\partial \mathbf{T}} \dot{\mathbf{T}} - \frac{\partial(L_{\mathbf{T}} \mathbf{g})}{\partial T_{des}} \dot{T}_{des} \\ &= \lambda^\top \mathbf{f}_{\mathbf{T}}(\mathbf{f}_{\mathbf{T}} \mathbf{g}) + L_{\mathbf{T}}(\mathbf{f}_{\mathbf{T}} \mathbf{g}) \\ &\quad - \left(\lambda^\top \frac{\partial(\mathbf{f}_{\mathbf{T}} \mathbf{g})}{\partial \mathbf{T}} + \frac{\partial(L_{\mathbf{T}} \mathbf{g})}{\partial \mathbf{T}} \right) \mathbf{f}(\mathbf{T}) \\ &\quad - \left(\lambda^\top \frac{\partial(\mathbf{f}_{\mathbf{T}} \mathbf{g})}{\partial T_{des}} + \frac{\partial(L_{\mathbf{T}} \mathbf{g})}{\partial T_{des}} \right) \dot{T}_{des} \\ &\quad - \left(\lambda^\top \frac{\partial(\mathbf{f}_{\mathbf{T}} \mathbf{g})}{\partial \mathbf{T}} + \frac{\partial(L_{\mathbf{T}} \mathbf{g})}{\partial \mathbf{T}} \right) \mathbf{g} \cdot \mathbf{u} \\ &= 0. \end{aligned} \quad (25)$$

Since all the necessary conditions must be satisfied for our solution to be optimal, we need to solve the system of (21), (24), and (25) simultaneously. This is a system of six equations with six unknowns, the inputs u_A , u_C , and the four adjoint states λ_i . One can easily notice that the solution of (21) and (24) can be done without solving (25). Equations (21) and (24) are also linear with respect to λ_i , so they have a unique solution. Then λ_i are substituted in (25) giving two equations linear in \mathbf{u} , that also give us a unique solution for \mathbf{u} as a function of \mathbf{T} and \dot{T}_{des} in the form,

$$\mathbf{u} = F(\mathbf{T}, \dot{T}_{des}). \quad (26)$$

Note that for implementation of this control law in the IMC structure (Fig. 4), the elements T_1 , T_2 , T_3 , of \mathbf{T} are replaced

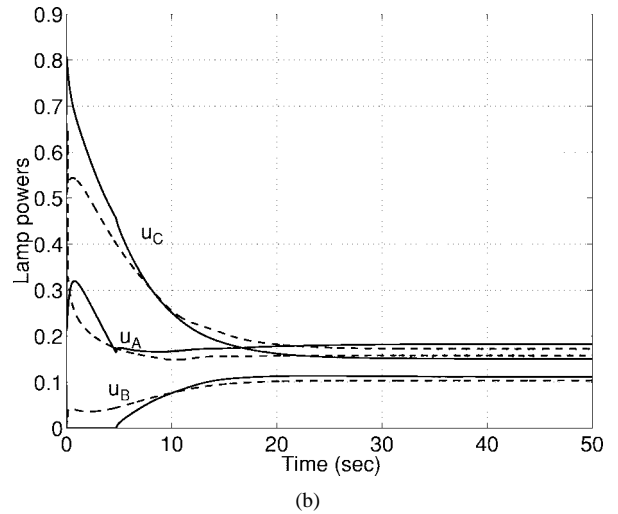
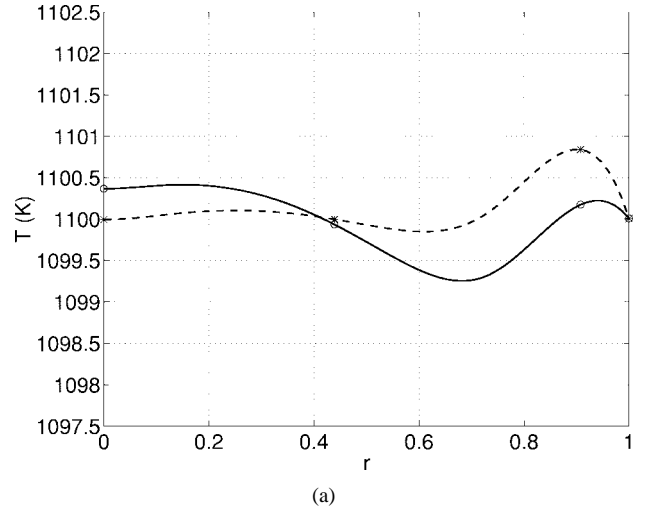


Fig. 9. IMC formulation using the full-order model as the simulated process with disturbance up to 10 K, varying wafer emissivity, and +40% chamber temperature, and the reduced-order model as the model. (a) Detailed temperature profile at $t = 50$ s and (b) manipulated inputs (lamp powers). Solid line: singular optimal control law. Dashed line: Hirschorn inverse.

by $T_{des} - (T_1 - \tilde{T}_1)$, $T_{des} - (T_2 - \tilde{T}_2)$, $T_{des} - (T_3 - \tilde{T}_3)$, respectively. \tilde{T}_c is used for the chamber temperature as the last element of \mathbf{T} . This is further illustrated in the next section.

This formulation is based on the simultaneous satisfaction of all the necessary optimality conditions and it is a static state feedback law. We denote with s the number of necessary time differentiations of the necessary optimality condition $H_{\mathbf{u}} = 0$ in order for \mathbf{u} to appear explicitly. Generalizing the singular optimal control theories presented in [10], one may identify s as the *degree of singularity* of the system. For our system $s = 2$. Then, we can state the following:

Theorem 1: For a multi-input system with k inputs, n states, and degree of singularity s , the singular trajectories can be tracked by static state feedback when

$$n = s \times k. \quad (27)$$

Proof: In order to obtain a static feedback law, the system of equations to be solved must be square. If the degree

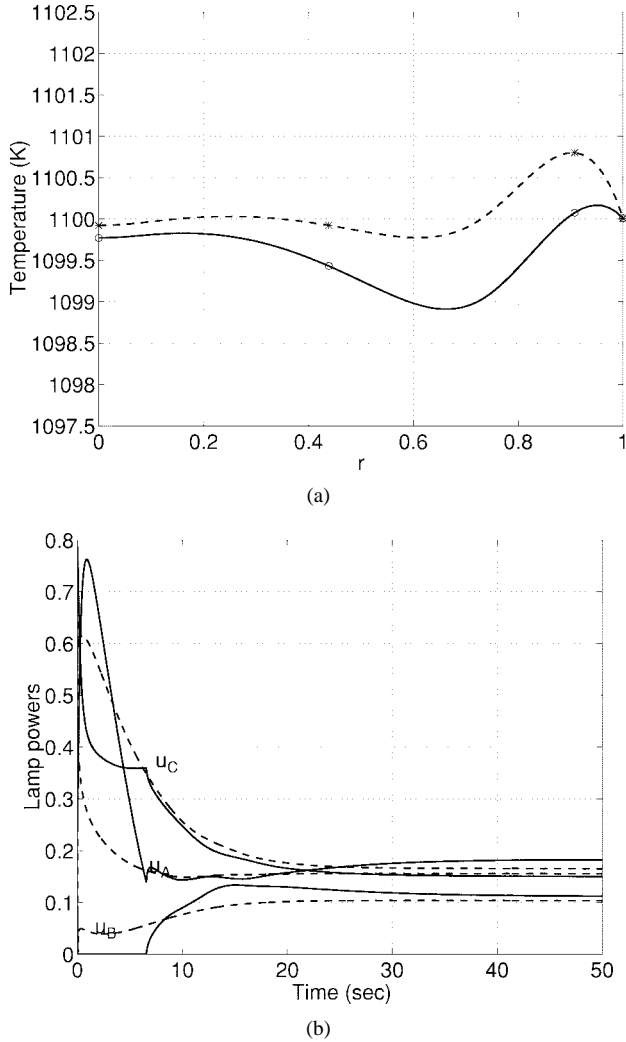


Fig. 10. IMC formulation using the full-order model as the simulated process with disturbance up to 50 K, varying wafer emissivity, and +40% chamber temperature, and the reduced-order model as the model. (a) Detailed temperature profile at $t = 50$ s and (b) manipulated inputs (lamp powers). Solid line: Singular optimal control law. Dashed line: Hirschorn inverse.

of singularity is s , the necessary optimality conditions will be

$$\begin{aligned} H_{\mathbf{u}} &= 0 \\ \frac{dH_{\mathbf{u}}}{dt} &= 0 \\ &\vdots \\ \frac{d^s H_{\mathbf{u}}}{dt^s} &= 0. \end{aligned} \quad (28)$$

Since \mathbf{u} is a $k \times 1$ vector system, (28) is a system of $(s+1) \times k$ equations. The inputs u_i will be the first k unknowns of the system. The remaining $s \times k$ unknowns are the adjoint states λ_i of the system. Since the number of adjoint states equals the number of states n , the system (28) is square only if $n = s \times k$. \square

We should note that the definition of the degree of singularity s as given in [10] has already made certain that the equations forming system (28) are linearly independent. Theorem 1 can be used for RTCVD temperature control

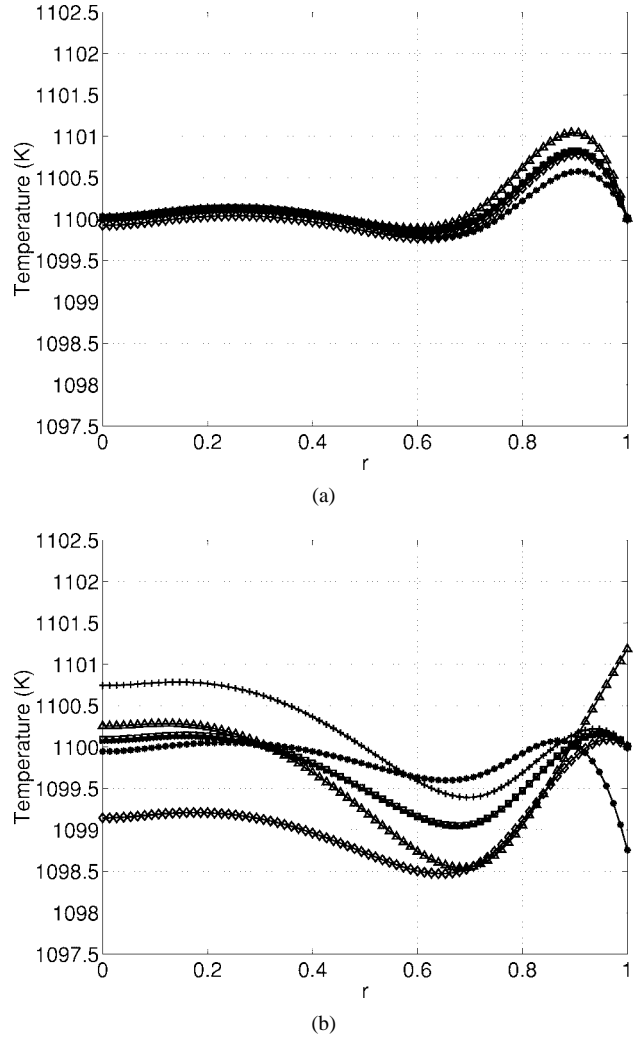


Fig. 11. Modified IMC structure using the full-order model as the simulated process with (a) Hirschorn inverse and (b) singular optimal controller with input uncertainty +15% or -15% in one input at each time. Detailed temperature profiles for $t = 50$ s. $\square, \triangle, \diamond$: +15% uncertainty in u_A, u_B, u_C . $\times, *, +$: -15% uncertainty in u_A, u_B, u_C .

problems with different number of inputs (lamp zones) and states (inner collocation points in the reduced-order model).

Finally, we should mention that a formulation of an extension to the constrained case can be found in [19]. However, since the values computed for u_A, u_C , during simulations by this algorithm (as well as Hirschorn's for that matter) never violated the lower and upper limits of zero and one, we have not included such a discussion here.

D. Comparison of the Two Control Laws

Fig. 5 illustrates how the two controllers are implemented in the IMC structure. One can also notice that the algebraic equation (10) is also implemented in the IMC structure in both cases as it was discussed in Section III-B.

Although the two structures in Fig. 5 look similar, there is a critical difference in addition to the number of inner points under control. For the implementation of the Hirschorn inverse in IMC, the time derivatives, not only of the setpoint, but also of the feedback $T_i - \hat{T}_i$, are needed, where T_i is the temperature

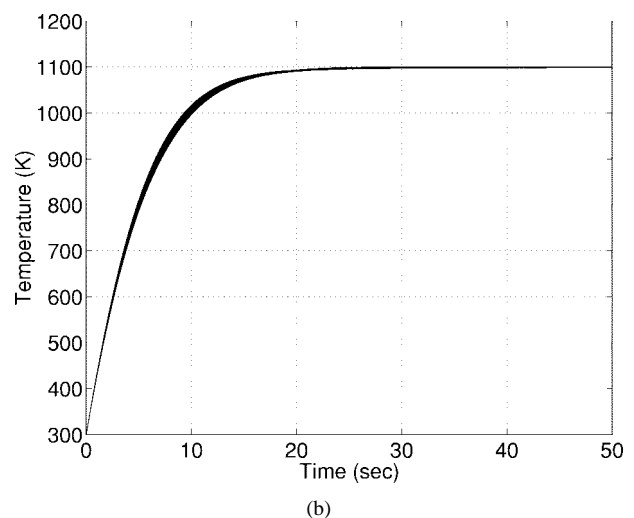
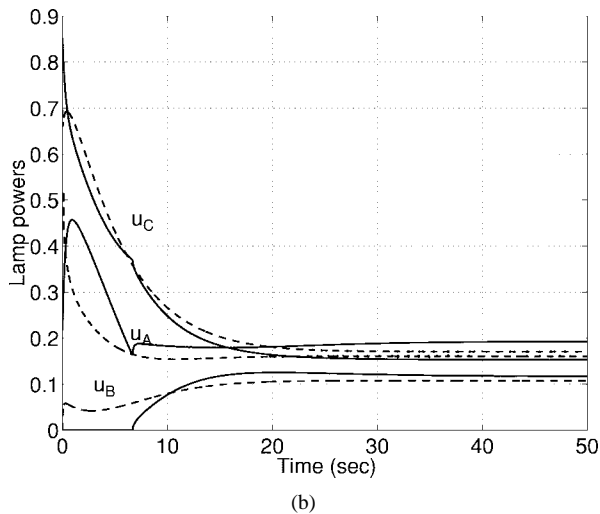
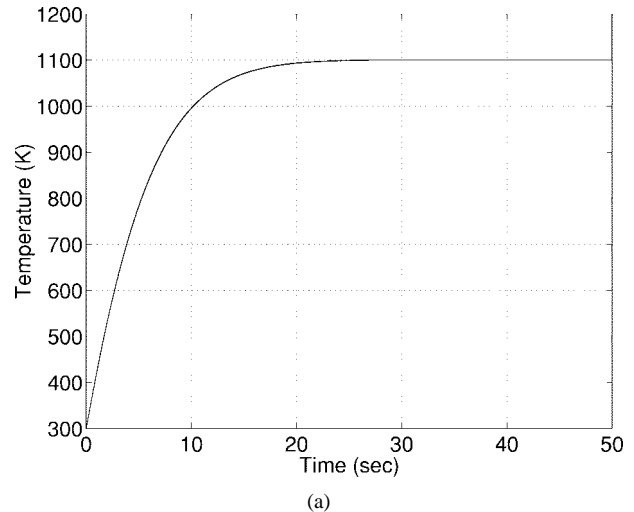
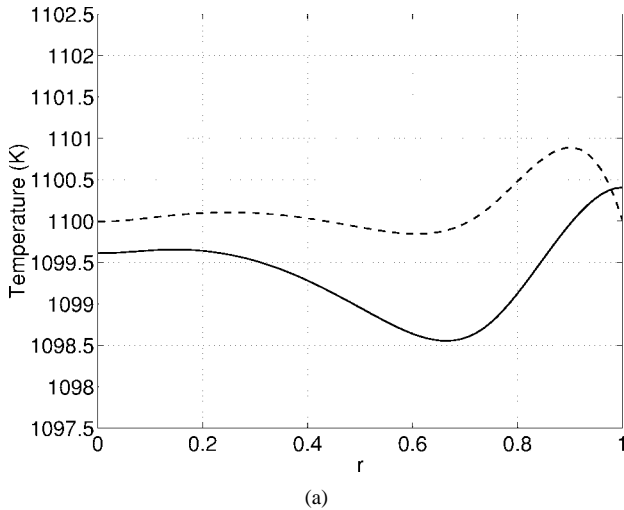


Fig. 12. Modified IMC structure using the full-order model as the simulated process with input uncertainty $+5\%$ at all inputs. (a) Detailed temperature profiles for $t = 50$ s and (b) manipulated inputs (lamp powers). Solid line: singular optimal control law. Dashed line: Hirschorn inverse.

Fig. 13. Modified IMC structure using the full-order model as the simulated process with input uncertainty $+5\%$ at all inputs. Dynamic response. (a) Hirschorn inverse and (b) singular optimal control law.

measurement of the process, and \tilde{T}_i the temperature estimated by the model. The calculation of the derivatives can only be done numerically, so a numerical error will be added to the calculations. In addition, the numerical calculation of this derivative will add computational effort to the estimation of the control inputs \mathbf{u} . Furthermore, if a system with relative order larger than one were considered, calculation of higher order derivatives would be involved, creating severe numerical errors.

This problem does not arise when the singular arc optimal controller (26) is used in the IMC structure, because in this case, only the setpoint time derivative needs to be evaluated. Since the setpoint is known *a priori*, the calculation of its derivative does not need to be done on-line, nor is it affected by measurement noise.

Furthermore, the Hirschorn inverse has no capability for handling the constrained case. On the contrary, the optimal control law can be suitably formulated to be applicable when a constraint becomes active. It should be noted, though, that none of the controllers can give anything more than the

suboptimal solution $u_B = 0$, in case the input u_B hits the lower constraint.

V. REAL-TIME CONTROL SIMULATIONS

In order to test the control theory presented in Section IV, as well as to implement the reduced-order model in a closed-loop scheme, we performed several simulations. We also considered several cases of uncertainty, some arising from the modeling of the system and others that might occur in the event of experimental validation.

Fig. 6 illustrates the dynamic simulation results of the modified IMC using as process P the full-order model and as model \tilde{P} the reduced-order model. The lines representing the 76 temperature discretization points of the full-order model are almost indistinguishable, showing that the desired temperature uniformity has been achieved. Furthermore, comparison of Fig. 6(a) with Fig. 2 indicates that we have also achieved setpoint tracking. A detail of the temperature profile at the final time of 50 s is shown in Fig. 7. The circles and the stars denote the collocation points. One may notice that, though the shape of the profiles across the wafer are different, the

uniformity achieved using either controller is within 1.2 K. This is definitely within the acceptable range recommended by the SIA Roadmap for Semiconductors [15], which calls for 5K maximum temperature nonuniformity.

A. Process Related Uncertainty

One might claim that the results in Fig. 7 are so good because the reduced-order model is such a good approximation of the process that the model-process mismatch is almost negligible. Thus, in order to check the robustness of the control scheme, a different simulation was performed, having as the process the full-order model with additive disturbance up to 10 K in each wafer temperature point. No disturbance is added to T_c . The disturbance is not only added to the simulated process output, but is also incorporated at each time step i of the numerical integration of the full-order model into the calculation of the state variables at $i + 1$. We can see that the effect of the disturbance on the quality of control is negligible, since the plots in Figs. 7 and 8 are the same up to the degree of the graph resolution. The same is also valid for the dynamic temperature profile and for this reason we omit presenting additional figures. We also notice that, as expected due to the IMC properties, there is no steady state offset for the Hirschorn inverse case for T_1 , T_2 , and T_4 that are directly controlled. Since the singular optimal controller is not an exact inverse of the model but minimizes (18), the setpoint tracking is not forced to be exact. We should also note that the plots of the temperatures include the additive disturbance, i.e., they would correspond to the true temperatures on the wafer.

We also performed a set of simulations considering parameter uncertainty. The way the process is described in [3], two parameters are not modeled precisely. One is the chamber temperature, which is described by the lumped equation (4). In reality, the chamber temperature is not constant throughout the surface of the chamber wall. It is, hence, a very difficult parameter to either measure or estimate. We performed simulations with up to $\pm 40\%$ multiplicative error in the chamber temperature T_c . The results look the same as in Figs. 6 and 7, up to the degree of the graph resolution.

The second parameter that is uncertain is the wafer emissivity ϵ_w . In [3], the emissivity is considered constant. In reality, the emissivity depends on the wafer temperature and the deposition thickness. Since the deposition thickness is also a function of the wafer temperature we cannot make the simulation more realistic, unless we solve the equations modeling the deposition thickness simultaneously with the wafer temperature dynamics. As an approximation, we did the following. We ran a simulation of the deposition thickness modeling equations presented in [3], using as the temperature dynamics the setpoint. Thus, we obtained the deposition thickness as a function of time. By polynomial fitting to the curves in Fig. 3 of [20] we have obtained ϵ_w as the following function of deposition thickness S :

$$\epsilon_w(S) = -70S^4 + 98S^3 - 41S^2 + 4.7S + 0.7 \quad (29)$$

where S has to be in μm . Substituting for S the dynamic profile we obtained by the simulated run, we have ϵ_w varying

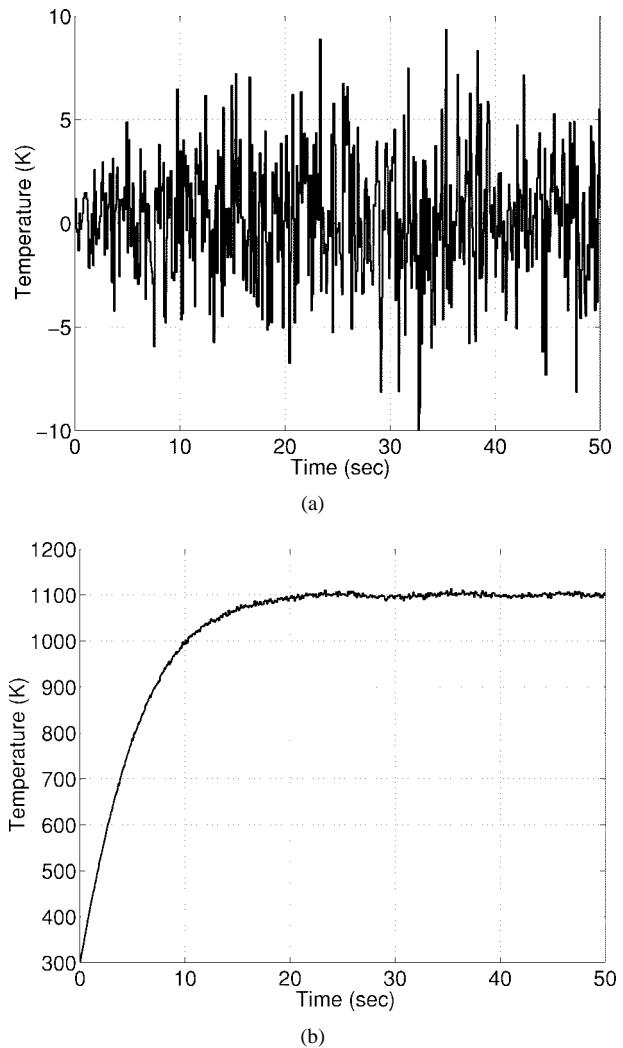


Fig. 14. (a) Measurement noise example and (b) edge temperature measurement with noise.

with time between 0.4738 and 0.8610. This is the emissivity we assume for our simulated process, while the model is based on constant emissivity $\epsilon_w = 0.7$. The results look, again, the same as in Figs. 6 and 7.

Fig. 9 presents the results of a simulated run including all the above mentioned types of error, i.e., process disturbance up to 10K, varying wafer emissivity, and +40% chamber temperature uncertainty. The temperature nonuniformity is well within the acceptable range. The plots show the final temperature profile across the wafer and the dynamic lamp power profiles during the run. The dynamic temperature profile is omitted as it looks, again, the same as in Fig. 6.

The same type of simulation is repeated with all these types of error present simultaneously, but the additive disturbance is increased to 50 K. (The disturbance starts from 0 at the beginning of the run and increases to the final value of 50 K with a speed similar to that of the desired temperature setpoint trajectory, i.e., it gets larger as the actual wafer temperature gets larger.) We can see from Fig. 10 that the uniformity is still kept within the acceptable range. The effect of different and larger types of error s can be seen more clearly

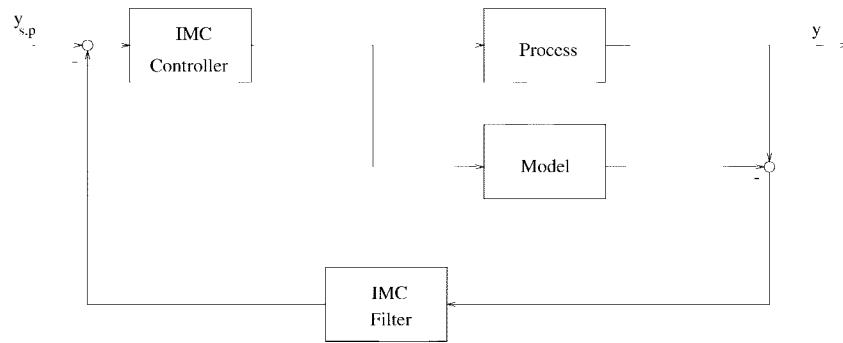


Fig. 15. IMC structure with filter at the feedback path.

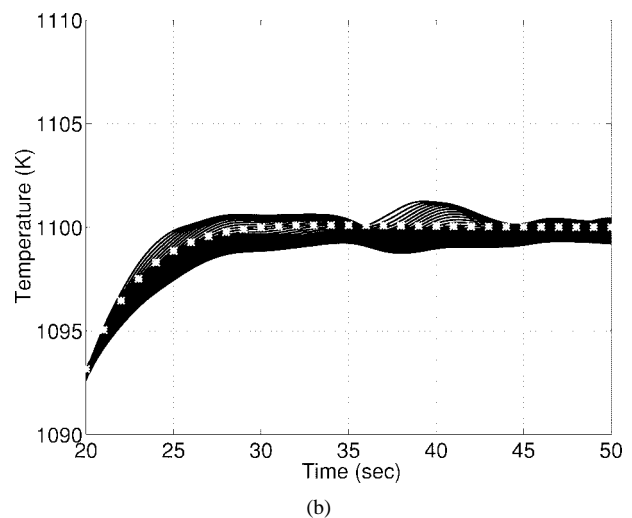
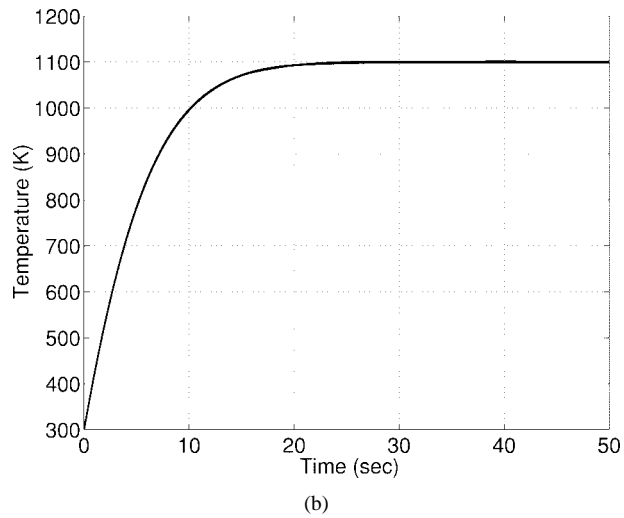
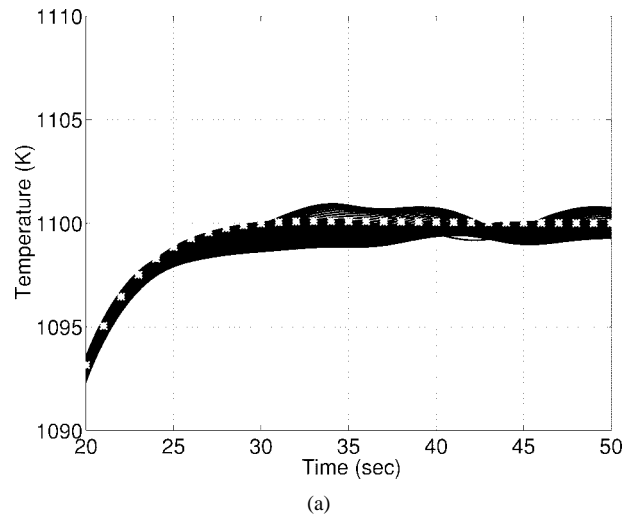
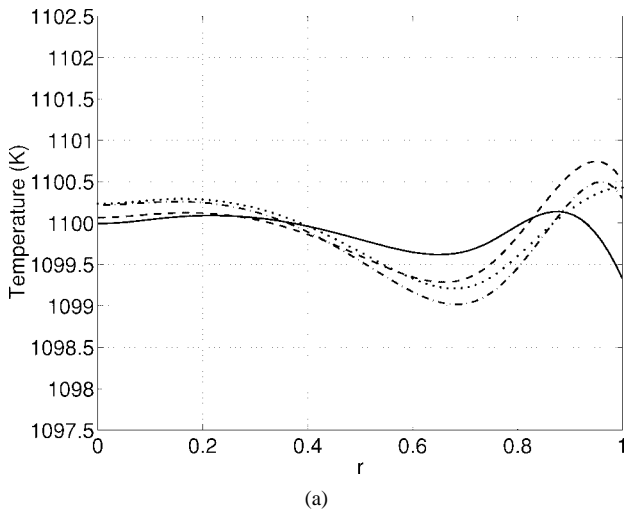


Fig. 16. IMC formulation with Gaussian measurement noise for the singular optimal control law. (a) Detailed final temperature profile using filter cutoff frequency $\omega_0 = 0.4$ (solid line), 0.6 (dashed), 0.8 (dash-dot), and 1 rad/s (dots). (b) Dynamic temperature profile with $\omega_0 = 1$ rad/s.

Fig. 17. IMC formulation with Gaussian measurement noise for the singular optimal control law. Dynamic temperature response detail with (a) $\omega_0 = 0.6$ rad/s and (b) $\omega_0 = 1$ rad/s. *: setpoint.

in the changes of the dynamic lamp power profiles that the controllers produce.

B. Actuator Uncertainty

A series of simulations was also performed involving actuator multiplicative errors in the range of $\pm 15\%$. This represents failure of the lamp bank power controls to follow precisely the

controller indications. Fig. 11 illustrates the final temperature profile of the cases $\pm 15\%$ uncertainty for one input at a time.

The results are different when all inputs are uncertain. Fig. 12 illustrates the results of a simulation performed with all three inputs having $+5\%$ multiplicative error. Note that the lamp power plots include the 5% error. We notice that the algorithm using the Hirschorn inverse works in this case better. This becomes more clear when comparing the dynamic

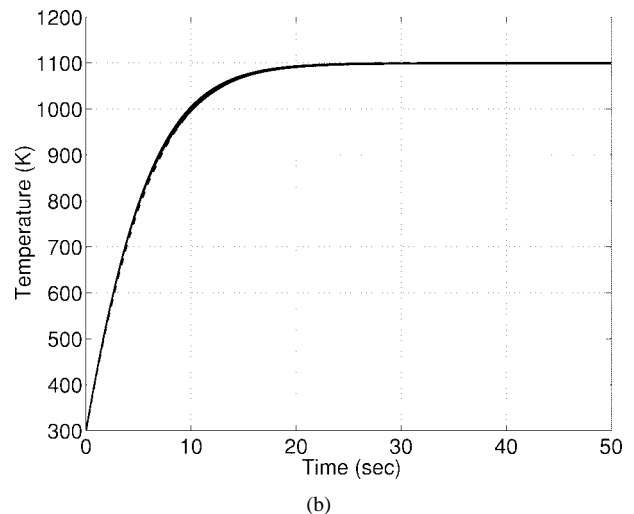
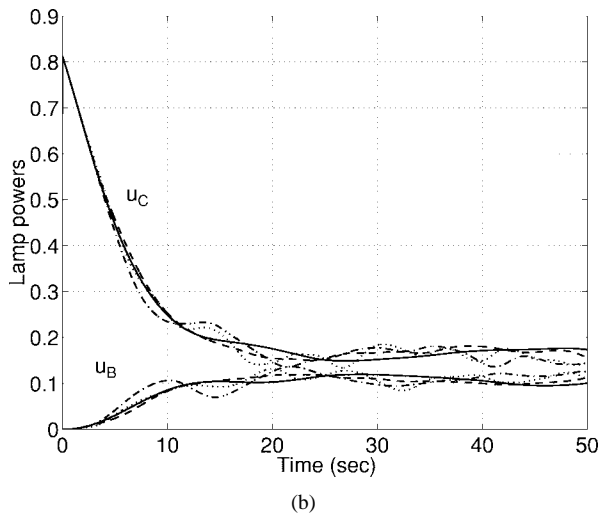
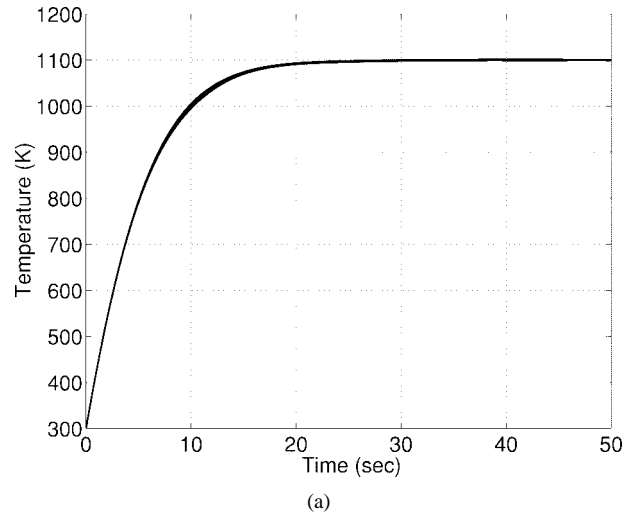
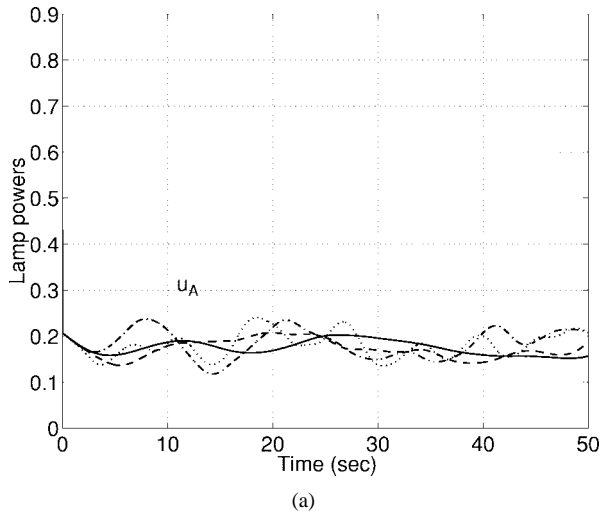


Fig. 18. IMC formulation with Gaussian measurement noise for the singular optimal control law. Power percentage of lamp banks using filter cutoff frequency $\omega_0 = 0.4$ (solid line), 0.6 (dashed), 0.8 (dash-dot), and 1 rad/s (dots).

Fig. 19. IMC formulation for the singular optimal control law with process related errors and filter of cutoff frequency $\omega_0 = 0.6$ rad/s (a) with measurement noise and (b) without noise.

profiles, shown in Fig. 13. At the beginning of the run, the controller fails to achieve temperature uniformity to the desirable degree, but this is corrected as time goes on. In all three simulations the full-order model was used to simulate the process.

C. The IMC Filter Design

In the case of measurement noise the feedback signal going to the IMC controller is not smooth, as it can be seen in Fig. 14. This is a Gaussian white noise signal scaled so that it is limited between -10 and 10 K. Due to the existence of noise, the performance of the IMC controller is not satisfactory, unless a filter is added. Especially in the case of the Hirschorn inverse, the calculation of the derivative of the feedback signal $T - \tilde{T} + \text{noise}$ is impossible due to numerical errors caused by the abrupt changes in the signal value. In this case, the existence of the filter in the feedback path is mandatory, in order to smooth out the effect of noise. The implementation of the IMC filter is shown in Fig. 15.

In the simulations we performed, we used a fourth order low-pass Butterworth filter [21]. The Butterworth filter is designed so that its magnitude squared function of the frequency is given by

$$|H|^2 = \frac{1}{1 + \left(\frac{\omega}{\omega_0}\right)^{2n}} \quad (30)$$

where ω_0 is the cutoff frequency, and n is the order of the filter. The transfer function $H(j\omega)$ has the following properties: it has n poles; all its zeros are at $\omega = \infty$; it has a bandwidth ranging from zero to ω_0 ; and its amplitude has value 1.0 at $\omega = 0$. This means that it is a type 1 filter [16], that is

$$H(0) = 1.$$

Due to a property of the IMC structure [12], since the filter is type 1, i.e., the steady state gain of the filter is 1, the closed loop system yields no offset at steady state, for asymptotically constant setpoints and disturbances.

The filter's cutoff frequency ω_0 has to be tuned in order for the filter to cut the noise, affecting as little as possible the

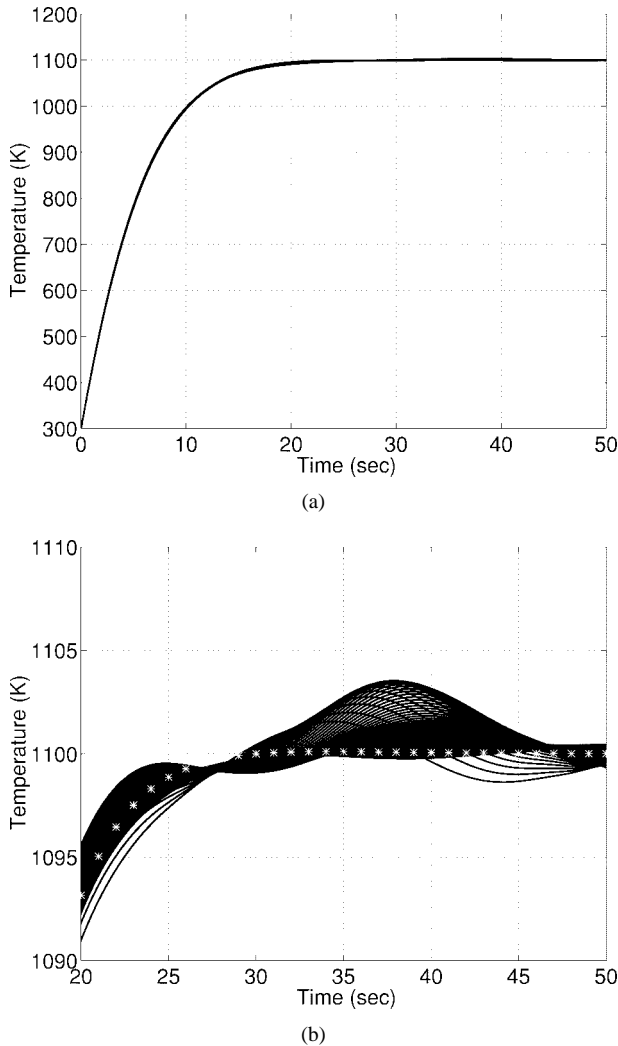


Fig. 20. IMC formulation with Gaussian measurement noise for the Hirschorn inverse with filter with $\omega_0 = 0.3$ rad/s. (a) Dynamic temperature response and (b) temperature response detail. *: setpoint.

measured process dynamics. In general, low cutoff frequencies improve the elimination of noise but, at the same time, the dynamics of the system are affected. On the other hand, high cutoff frequencies leave the system dynamics unaffected but do not smooth out the noise effectively. Hence, in the tuning procedure a compromise between performance and robustness is necessary proving an intermediate cutoff frequency range to be optimal. The tuning procedure indicated that the Hirschorn inverse is more sensitive to noise, as expected due to the differentiation of the measurements, thus requiring a lower cutoff frequency.

For the tuning of the singular optimal control law, cutoff frequencies between 0.4 and 1 rad/s were tested. Simulation results are demonstrated in the following figures. In all simulations the full-order model is used to emulate the process. The plots of the temperatures correspond to what would be the true temperatures, prior to the addition of the measurement noise. The feedback control signals include the noise of course. In Fig. 16(a) the detailed final time profiles of the actual temperatures are shown when there is measurement noise. Although all noise profiles are Gaussian white noise as the

signal in Fig. 14(a), a different seed is used to generate the noise added to each temperature measurement. We notice that the final temperature profile tends to be closer to the one of the corresponding simulation without noise (Fig. 7) for the cutoff frequencies between 0.6 and 0.8 rad/s. At the same time, though, the noise elimination gets worse. This does not show in Fig. 16 where the 76 temperature curves essentially overlap. It hardly starts showing in Fig. 17 where a detail of the temperature dynamics is presented. It becomes more obvious, though, if one examines the lamp powers in Fig. 18, which become more oscillatory as the cutoff frequency increases.

Fig. 19 illustrates the use of the IMC filter in the presence of process related errors, same as in Fig. 9. We use cutoff frequency $\omega_0 = 0.6$ rad/s since it eliminates the noise sufficiently and does not affect severely the dynamics of the process as this is indicated in Fig. 19(b) with the good matching of the setpoint (dashed line) to the 76 temperature curves.

The tuning procedure for the Hirschorn inverse confirmed the increased sensitivity of this controller to measurement noise. The range of cutoff frequencies tested in the singular optimal controller was not sufficient. The final cutoff frequency we decided upon was $\omega_0 = 0.3$ rad/s. As we can see in Fig. 20, and even more clearly from the lamp power plots in Fig. 21, there is still oscillation. Also, in Fig. 22 we can see that the IMC filter with $\omega_0 = 0.3$ rad/s affects severely the dynamics of the closed-loop system in the case of process uncertainty and disturbances. In this simulation, the same process related errors are used as in Figs. 19(b) and 9.

VI. CONCLUSIONS

Two model-based real-time control algorithms were successfully developed for controlling temperature uniformity on the wafer surface for a three-zone RTCVD reactor. A reduced-order model describing the distributed parameter system is utilized by the controllers. The development was done within the nonlinear IMC structure, which was modified specifically to deal with systems described by differential-algebraic equations. It was necessary to extend the optimal control theory for singular arcs to multi-input systems, contributing also in the area of control of nonlinear nonsquare systems that are affine in the inputs. Both the singular optimal controller and the one based on the Hirschorn inverse of the model were extensively tested for robustness to process uncertainty, disturbances and measurement noise. They were shown to demonstrate robust behavior, though, as it was expected, the Hirschorn inverse cannot handle measurement noise as efficiently as the singular optimal controller. The simulation results are very encouraging. In particular, the successful robustness tests indicate that the implementation of the proposed real-time model based control algorithms on RTCVD systems allows one to control uniformity within the goals set by the SIA National Technology Roadmap for Semiconductors [15].

Finally, it should be noted that both controller design procedures allow a certain degree of flexibility as to which points on the wafer are controlled, depending on the available temperature measurements. If measurements of the edge temperature are unavailable, then all three inputs (lamp powers)

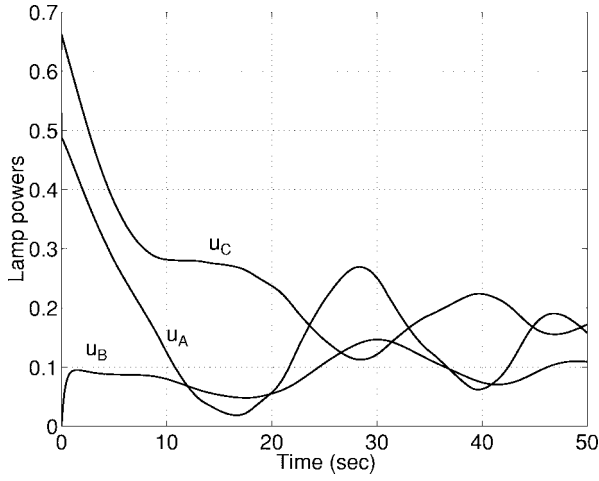


Fig. 21. IMC formulation with Gaussian measurement noise for the Hirschorn inverse. Manipulated inputs for $\omega_0 = 0.3$ rad/s.

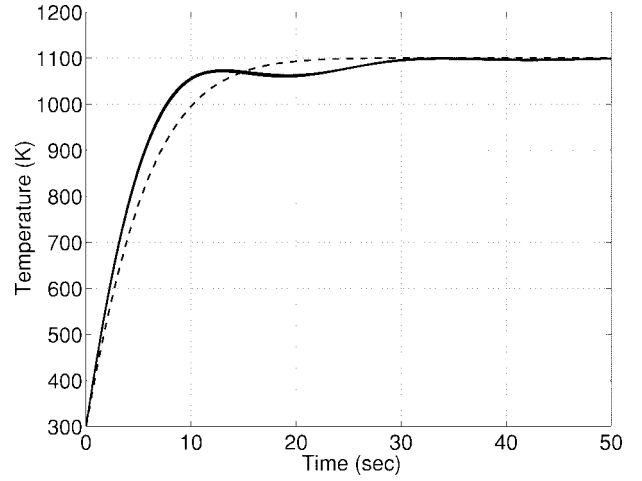
can be used to control the three inner points via the Hirschorn inverse controller. In such a case, for the singular optimal controller, Theorem 1 would allow the use for a reduced-order model with more inner collocation points, subject to satisfaction of (27), and the temperatures of these points could be included in the objective function of the optimization.

APPENDIX

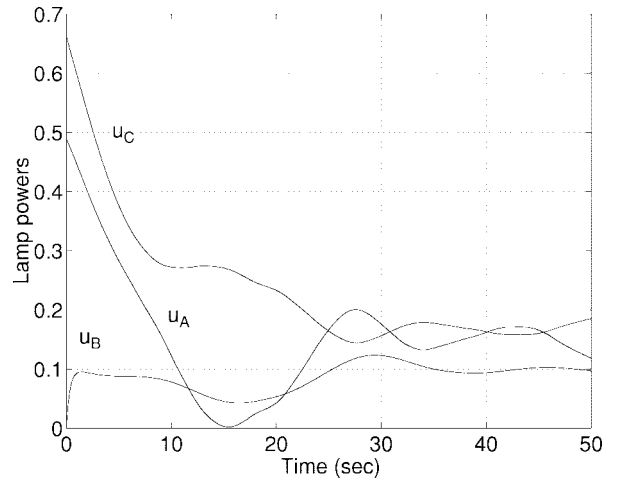
The reduced-order model is expressed in the form

for $i = 1, \dots, 3$

$$\begin{aligned} & \rho_w \left[\frac{dC_{p_w}}{dT} \Big|_{T=T_i} T_i + C_{p_w}(T_i) \right] \frac{dT_i}{dt} \\ &= \frac{1}{R_w^2} \left[\frac{d\kappa}{dT} \Big|_{T=T_i} (\mathbf{A} \cdot \mathbf{T})_i^2 + \kappa(\mathbf{B} \cdot \mathbf{T})_i \right] \\ &+ \frac{1}{T_{amb} \delta z} [\mathbf{Q}_{lamps, w}(r_i) \cdot \mathbf{u} + q_{dw, b}(r_i) + q_{dw, t}(r_i)] \end{aligned} \quad (31)$$



(a)



(b)

Fig. 22. IMC formulation for the Hirschorn inverse with process related errors and filter of cutoff frequency $\omega_0 = 0.3$ rad/s, with Gaussian measurement noise. (a) Solid lines: dynamic temperature response; dashed line: setpoint. (b) Manipulated inputs (lamp powers).

$$\begin{aligned} \mathbf{A} &= \begin{bmatrix} 0 & 0 & 0 & 0 \\ -0.987897 & -0.112753 & 1.69256 & -0.591905 \\ 0.147480 & -1.85294 & -3.70189 & 5.40735 \\ 5.63929 & -4.85669 & -19.8083 & 19.0257 \end{bmatrix} \\ \mathbf{B} &= \begin{bmatrix} -3.26828 & -0.0762699 & 6.14695 & -2.80240 \\ -4.84154 & -0.717501 & 7.99073 & -2.43170 \\ 31.8788 & -20.8281 & -99.7517 & 88.7011 \\ 104.272 & -58.0574 & -307.702 & 261.488 \end{bmatrix} \\ \mathbf{\Psi} &= \begin{bmatrix} 1 & 1.36681 & -0.807549 \\ 1 & 0.931689 & 0 \\ 1 & -1.02275 & 0 \\ 1 & -1.69066 & -4.95123 \end{bmatrix} \\ \mathbf{Q}_{lamps, w} &= \begin{bmatrix} 9.1 & 8.91325 & 7.49502 & 7 \\ 0.9 & 1.03157 & 3.12009 & 4 \\ 17 & 17.1378 & 17.4292 & 17.5000 \end{bmatrix} \end{aligned} \quad (33)$$

with boundary condition

$$\frac{\kappa(T_4)T_{amb}}{R_w} (\mathbf{A} \cdot \mathbf{T})_4 = -\sigma\epsilon_w T_{amb}^4 (T_4^4 - T_c^4) + q_{edge} u_B \quad (32)$$

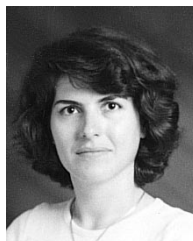
where $(\mathbf{A} \cdot \mathbf{T})_i$ and $(\mathbf{B} \cdot \mathbf{T})_i$ are the i th elements of the vectors $(\mathbf{A} \cdot \mathbf{T})$ and $(\mathbf{B} \cdot \mathbf{T})$, respectively.

The chamber temperature equation, as well as detailed explanation and values for the several terms in (31) and (32) are given in [3]. The discretization matrices for the four-point reduced-order model are shown in (33), at the bottom of the previous page.

REFERENCES

- [1] E. Zafiriou, H.-W. Chiou, and R. A. Adomaitis, "Nonlinear model based run-to-run control for rapid thermal processing with unmeasured variable estimation," in *Symp. Control, Diagnostics and Modeling in Semiconductor Manufacturing, 187th Meeting Electrochem. Soc.*, M. Meyyappan, D. J. Economou, and S. W. Butler, Eds., Reno, NV, May 1995, vol. 95-2, pp. 18–31.
- [2] T. Breedijk, T. F. Edgar, and I. Trachtenberg, "A model predictive controller for multivariable temperature control in rapid thermal processing," in *Proc. Amer. Control Conf.*, San Francisco, CA, June 1993, pp. 2990–2984.
- [3] A. Theodoropoulou, R. A. Adomaitis, and E. Zafiriou, "Model reduction for optimization of rapid thermal chemical vapor deposition systems," *IEEE Trans. Semiconduct. Manufact.*, vol. 11, pp. 85–98, Feb. 1998.
- [4] Y. M. Cho and P. Gyugyi, "Control of rapid thermal processing: A system theoretic approach," *IEEE Trans. Control Syst. Technol.*, vol. 5, pp. 644–653, Nov. 1997.
- [5] P. Spence, C. Schapper, and A. Kermani, "Concurrent design of an rtp chamber and advanced control system," in *Symp. Rapid Thermal and Integrated Processing IV*, S. R. J. Brueck, J. C. Gelpey, A. Kermani, J. L. Regolini, and J. C. Sturm, Eds., Mater. Soc., San Francisco, CA, Apr. 1995, vol. 387, pp. 75–86.
- [6] W. J. Kiether, M. T. Fordham, S. Yu, A. J. S. Neto, K. A. Conrad, J. R. Hauser, F. Y. Sorrell, and J. J. Wortman, "Three-zone rapid thermal processor system," in *Proc. 2nd Int. RTP Conf.*, Monterey, CA, 1994, pp. 96–100.
- [7] M. Rouff and F. Lamnabhi-Lagarrigue, "A new approach to nonlinear optimal feedback law," *Syst. Contr. Lett.*, vol. 7, pp. 411–417, 1986.
- [8] J. M. Modak and H. C. Lim, "Feedback optimization of fed-batch fermentation," *Biotechnol. Bioeng.*, vol. XXX, pp. 528–540, 1987.
- [9] ———, "Simple nonsingular control approach to fed-batch fermentation optimization," *Biotechnol. Bioeng.*, vol. 33, pp. 11–15, 1989.
- [10] S. Palanki, C. Kravaris, and H. Y. Wang, "Synthesis of state feedback laws for end point optimization in batch processes," *Chem. Eng. Sci.*, vol. 48, no. 1, pp. 135–151, 1993.
- [11] R. M. Hirschorn, "Invertibility of nonlinear control systems," *SIAM J. Contr. Optim.*, vol. 17, pp. 289–297, 1979.
- [12] C. G. Economou, M. Morari, and B. O. Palsson, "Internal model control. 5. extension to nonlinear systems," *Ind. Eng. Chem. Process Des. Dev.*, vol. 25, pp. 403–411, 1986.
- [13] L. L. Tedder, G. W. Rubloff, I. Shareef, M. Anderle, D.-H. Kim, and G. N. Parsons, "Real-time process and product diagnostics in rapid thermal chemical vapor deposition using *in situ* mass spectrometric sampling," *J. Vac. Sci. Technol. B*, vol. 13, pp. 1924–1927, July/Aug. 1995.
- [14] J. V. Villadsen and W. E. Stewart, "Solution of boundary-value problems by orthogonal collocation," *Chem. Eng. Sci.*, vol. 22, pp. 1483–1501, 1967.
- [15] The Semiconductor Industry Association, *The National Technology Roadmap for Semiconductors*, San Jose, CA, 1994.
- [16] M. Morari and E. Zafiriou, *Robust Process Control*. Englewood Cliffs, NJ: Prentice-Hall, 1989.
- [17] C. Kravaris and J. C. Kantor, "Geometric methods for nonlinear process control. 1. Background," *Ind. Eng. Chem. Res.*, vol. 29, pp. 2295–2309, 1990.
- [18] A. E. Bryson and Y.-C. Ho, *Applied Optimal Control*. Washington, DC: Hemisphere, 1975.

- [19] A. Theodoropoulou, "Model reduction and temperature uniformity control for rapid thermal chemical vapor deposition reactors," Ph.D. dissertation, Univ. Maryland, College Park, 1997.
- [20] F. Y. Sorrell, J. A. Harris, and R. S. Gyurcsik, "A global model for rapid thermal processors," *IEEE Trans. Semiconduct. Manufact.*, vol. 3, pp. 183–188, Nov. 1990.
- [21] G. F. Franklin and D. J. Powell, *Digital Control of Dynamic Systems*. Reading, MA: Addison-Wesley, 1980.



Artemis Theodoropoulou received the Diploma in chemical engineering in 1992 from the University of Patras, Patras, Greece, and the Ph.D. degree in 1997, also in chemical engineering, in the area of process control, from the University of Maryland, College Park.

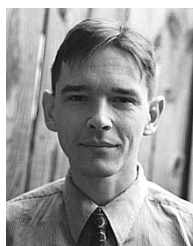
She became a Graduate Research Assistant at the Institute for Systems Research (ISR), University of Maryland in 1992. Currently, she is with OSI Software, Inc. (formerly Oil Systems, Inc.), San Leandro, CA. Her current work involves the development of real-time data acquisition and industrial process data storage software. Her interests also include modeling, simulation, model reduction, optimization and process control.



Evangelhos Zafiriou (M'88) received the Diploma in chemical engineering in 1983 from the National Technical University, Athens, Greece, and the Ph.D. degree, also in chemical engineering, from the California Institute of Technology, Pasadena, in 1987.

He then joined the faculty of the University of Maryland, College Park, where he currently holds a joint appointment as an Associate Professor with the Department of Chemical Engineering and the Institute for Systems Research. His research interests are in the area of process control, optimization, and model identification, covering both theory and applications in the chemical, oil, and semiconductor manufacturing industries. He has coauthored a graduate level textbook, *Robust Process Control* (Englewood Cliffs, NJ: Prentice-Hall, 1989) and has lectured nationally and internationally at short courses for the industry. He has served as editor/coeditor of the proceedings of three international meetings and has been involved in organizing more than 20 national and international meetings and sessions.

Dr. Zafiriou is a recipient of a 1990 NSF Presidential Young Investigator Award and a Member of AIChE, ACS, and SIAM.



Raymond A. Adomaitis received the B.S. and Ph.D. degrees in chemical engineering from the Illinois Institute of Technology, Chicago, in 1984 and 1988, respectively.

He then took a postdoctoral research associateship in the Chemical Engineering Department of Princeton University, Princeton, NJ, and then joined the University of Maryland, first as Postdoctoral Fellow from 1990 to 1992, and then as a Research Faculty Member from 1992 to 1995. He is currently an Assistant Professor of chemical engineering, with a joint appointment in the Institute for Systems Research (ISR), University of Maryland. He also serves as the Director of the Computer Aided Control Systems Engineering Laboratory in the ISR. His research focuses on the development of numerical and computational techniques for modeling, model reduction, and simulation of distributed parameter systems with applications in electronic materials manufacturing processes.